https://doi.org/10.1016/j.cmet.2018.07.019

Impairment of Angiogenesis by Fatty Acid Synthase Inhibition Involves mTOR Malonylation

Graphical Abstract

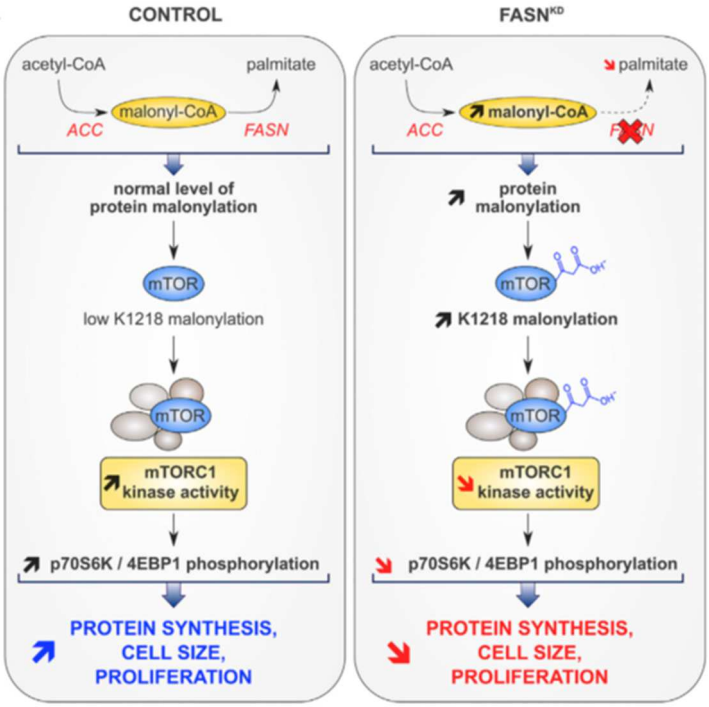

Authors

Ulrike Bruning, Francisco Morales-Rodriguez, Joanna Kalucka, ..., Xuri Li, Massimiliano Mazzone, Peter Carmeliet

Correspondence

lixr6@mail.sysu.edu.cn (X.L.), peter.carmeliet@kuleuven.vib.be (P.C.)

In Brief

Bruning et al. report that blocking fatty acid synthase (FASN) in endothelial cells (ECs) reduces angiogenesis by impairing EC proliferation. Mechanistically, FASN inhibition elevates the malonyl-CoA substrate pool, thereby increasing posttranslational malonylation of mTOR and decreasing the pro-angiogenic mTORC1 activity.

Highlights

- Fatty acid synthase inhibition impairs physiological and pathological angiogenesis
- FASN inhibition selectively reduces endothelial cell proliferation, not migration
- By elevating malonyl-CoA levels, FASN inhibition promotes mTOR lysine malonylation
- The resultant decrease in mTORC1 kinase activity contributes to angiogenic defects

https://doi.org/10.1016/j.cmet.2018.07.019

Impairment of Angiogenesis by Fatty Acid Synthase Inhibition Involves mTOR Malonylation

Ulrike Bruning,[1,2,3,17] Francisco Morales-Rodriguez,[1,3,17] Joanna Kalucka,[1,3] Jermaine Goveia,[1,3] Federico Taverna,[1,3] Karla C.S. Queiroz,[1,3] Charlotte Dubois,[1,3] Anna Rita Cantelmo,[1,3] Rongyuan Chen,[2] Stefan Loroch,[4] Evy Timmerman,[5,6,7] Vanessa Caixeta,[4] Katarzyna Bloch,[8] Lena-Christin Conradi,[1,3] Lucas Treps,[1,3] An Staes,[5,6,7] Kris Gevaert,[5,6,7] Andrew Tee,[9] Mieke Dewerchin,[1,3] Clay F. Semenkovich,[10] Francis Impens,[5,6,7] Birgit Schilling,[11] Eric Verdin,[11] Johannes V. Swinnen,[8] Jordan L. Meier,[12] Rhushikesh A. Kulkarni,[12] Albert Sickmann,[4] Bart Ghesquie` re,[13,14] Luc Schoonjans,[1,2,3] Xuri Li,[2,*] Massimiliano Mazzone,[15,16] and Peter Carmeliet[1,2,3,18,*]

[1]Laboratory of Angiogenesis and Vascular Metabolism, VIB Center for Cancer Biology (CCB), VIB, 3000 Leuven, Belgium
[2]StateKey Laboratory of Ophthalmology, Zhongshan Ophthalmic Center, SunYat-Sen University,Guangzhou 510060,Guangdong, P.R. China
[3]Laboratory of Angiogenesis and Vascular Metabolism, Department of Oncology and Leuven Cancer Institute (LKI), KU Leuven, 3000 Leuven,
Belgium
[4]Leibniz Institut f€ur analytische Wissenschaften, ISAS, 44227 Dortmund, Germany
[5]VIB Center for Medical Biotechnology, 9000 Ghent, Belgium
[6]Department of Biochemistry, Ghent University, 9000 Ghent, Belgium
[7]VIB Proteomics Expertise Center, 9000 Ghent, Belgium
[8]Laboratory of Lipid Metabolism and Cancer, Department of Oncology, KU Leuven, 3000 Leuven, Belgium
[9]Cardiff University, Cardiff CF14 4YS, UK
[10]Division of Endocrinology, Metabolism & Lipid Research, Washington University, St. Louis, MO 63110, USA
[11]Buck Institute for Research on Aging, Novato, CA 94945, USA
[12]National Cancer Institute, Frederick, MD 21702, USA
[13]Metabolomics Core Facility, Department of Oncology, KU Leuven, 3000 Leuven, Belgium
[14]Metabolomics Core Facility, VIB Center for Cancer Biology (CCB), VIB, 3000 Leuven, Belgium
[15]Laboratory of Tumor Inflammation and Angiogenesis, VIB Center for Cancer Biology (CCB), VIB, 3000 Leuven, Belgium
[16]Laboratory of Tumor Inflammation and Angiogenesis, Department of Oncology, KU Leuven, 3000 Leuven, Belgium
[17]These authors contributed equally
[18]Lead Contact

*Correspondence: lixr6@mail.sysu.edu.cn (X.L.), peter.carmeliet@kuleuven.vib.be (P.C.)
https://doi.org/10.1016/j.cmet.2018.07.019

SUMMARY

The role of fatty acid synthesis in endothelial cells (ECs) remains incompletely characterized. We report that fatty acid synthase knockdown ($FASN_{KD}$) in ECs impedes vessel sprouting by reducing proliferation. Endothelial loss of FASN impaired angiogenesis in vivo, while FASN blockade reduced pathological ocular neovascularization, at >10-fold lower doses than used for anti-cancer treatment. Impaired angiogenesis was not due to energy stress, redox imbalance, or palmitate depletion. Rather, $FASN_{KD}$ elevated malonyl-CoA levels, causing malonylation (a post-translational modification) of mTOR at lysine 1218 (K1218). mTOR K-1218 malonylation impaired mTOR complex 1 (mTORC1) kinase activity, thereby reducing phosphorylation of downstream targets (p70S6K/4EBP1). Silencing acetyl-CoA carboxylase 1 (an enzyme producing malonyl-CoA) normalized malonyl-CoA levels and reactivated mTOR in $FASN_{KD}$ ECs. Mutagenesis unveiled the importance of mTOR K1218 malonylation for angiogenesis. This study unveils a novel role of FASN in metabolite signaling that contributes to explaining the anti-angiogenic effect of FASN blockade.

INTRODUCTION

Fatty acid synthase (FASN) mediates de novo lipid synthesis by catalyzing the production of palmitate from acetyl-coenzyme A (CoA), malonyl-CoA, and NADPH. Palmitate is used for the synthesis of more complex fatty acids (FAs), plasma membrane structures, and post-translational protein palmitoylation (Rohrig and Schulze, 2016). In contrast to most non-transformed cells, which satisfy their demand from dietary lipids, cancer cells often synthesize up to 95% of FAs de novo despite sufficient dietary supply (Zaidi et al., 2013). Not surprisingly, lipogenesis has been implicated in cancer cell biology (Rohrig and Schulze, 2016).

Limited evidence has implicated FASN in angiogenesis. In vitro, the FASN blocker orlistat inhibits EC proliferation, associated with downregulation of vascular endothelial growth factor receptor 2 (Browne et al., 2006), but it is unknown whether the latter is cause or consequence of FASN inhibition. Constitutive FASN loss in ECs and hematopoietic cells decreases angiogenesis in ischemia (Wei et al., 2011). Nonetheless, the role of endothelial FASN loss in physiological development in vivo has not been studied, neither the therapeutic potential of FASN blockade in pathological ocular angiogenesis.

Malonyl-CoA participates in (patho-)physiological processes (Saggerson, 2008). While FASN inhibition impaired palmitoylation due to reduced palmitate synthesis (Wei et al., 2011),

https://doi.org/10.1016/j.cmet.2018.07.019

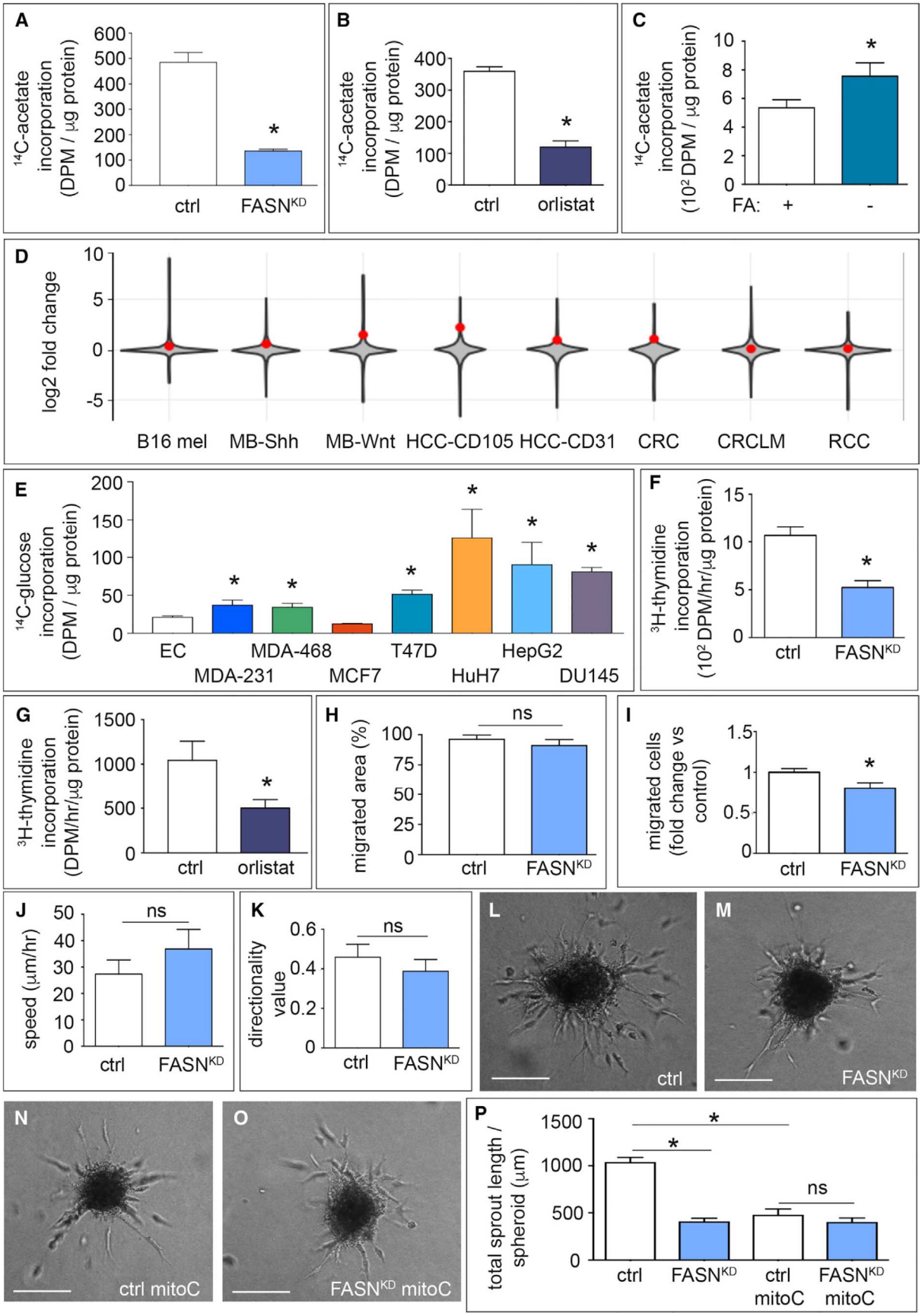

https://doi.org/10.1016/j.cmet.2018.07.019

Figure 1. Role of Endothelial Fatty Acid Synthase in Vessel Sprouting
(A and B) Incorporation of carbons from [U-^{14}C]-acetate in the fatty acid (FA) fraction of control (ctrl) and FASN$_{KD}$ ECs (n = 3) (A) or control and orlistat-treated (10 mM) ECs (n = 4) (B). DPM, disintegrations per minute.
(C) Incorporation of carbons from [U-^{14}C]-acetate in the FA fraction of ECs in the presence or absence of FAs in the medium (n = 3). DPM, disintegrations per minute.
(D) Violin plots visualizing the log$_2$ fold-change distribution in gene expression (gray area) in murine and human tumor ECs versus their counterpart normal healthy ECs. The red dot indicates where FASN is located in the distribution. Data are based on a meta-analysis of publicly available transcriptome datasets of murine B16 melanoma (B16 mel); murine medulloblastoma (MB-Shh, MB-Wnt); human hepatocellular carcinoma (HCC-CD105, HCC-CD31); human colorectal cancer (CRC, CRCLM) and human renal cancer (RCC). p = 1.0 3 10_20 (Fisher's method).
(E) Incorporation of carbons from [U-^{14}C]-glucose in the FA fraction of ECs (EC), breast cancer cell lines MDA-MB-231 (MDA-231), MDA-MB-468 (MDA-468), T47D, and MCF7, hepatocellular carcinoma cells HuH7 and HepG2, and prostate cancer cells DU145 in their optimal growth medium (n = 3). DPM, disintegrations per minute.
(F and G) [^{3}H]-Thymidine incorporation into DNA (proliferation assay) in control and FASN$_{KD}$ ECs (n = 4) (F), and in control or orlistat-treated ECs (n = 5) (G). DPM, disintegrations per minute.
(H) Scratch wound migration assay using mitotically inactivated (mitoC) control or FASN$_{KD}$ ECs (n = 3).
(I) Number of mitoC-treated control and FASN$_{KD}$ ECs that traversed the membrane in a Boyden chamber (expressed relative to control; n = 3).
(J and K) Analysis of random cell-motility tracks obtained by time-lapse imaging of GFP$_+$ ECs (transduced with a lentiviral vector expressing GFP), for speed (J) or directional persistence of EC movement (K) in control and FASN$_{KD}$ ECs (n = 4).
(L–O) Representative phase-contrast images of EC spheroids of proliferating (L and M) and mitotically inactivated ECs (mitoC) (N and O) using control (L and N) or FASN$_{KD}$ ECs (M and O). Scale bars, 200 mm.
(P) Total sprout length of control and FASN$_{KD}$ EC spheroids with and without mitotic inactivation (mitoC) (n = 3). Data are mean ± SEM. *p < 0.05 by Fisher's combined probability test (D) and mixed models statistics for all other panels. ns, not significant. See also Figure S1.

consequences of elevated levels of malonyl-CoA as a result of FASN inhibition in ECs were not considered. Malonyl-CoA can be non-enzymatically used for protein lysine malonylation, a recently identified post-translational modification (PTM) that can alter protein activity (Peng et al., 2011). Even though protein malonylation is evolutionarily conserved from bacteria to mammals, the functional consequences and stoichiometry of this PTM are poorly characterized (Du et al., 2015; Nishida et al., 2015), and have never been determined in a single study. Here, we explored whether FASN might regulate angiogenesis via malonylation of key targets.

RESULTS

Fatty Acid Synthesis in Endothelial Cells

We explored whether human umbilical venous ECs (referred to hereafter as ECs) synthesized palmitate de novo. To mimic in vivo physiological conditions, we used physiological concentrations of palmitate (100–120 mM), acetate (200–500 mM), and glucose (5.5 mM) and added trace amounts of ^{14}C-labeled acetate (<0.1% of the concentration of the cold acetate). When quantifying the incorporation of labeled carbons into the FA fraction, we detected measurable levels of FA synthesis in ECs, despite available palmitate in the medium (Figures 1A and 1B).

To assess whether this signal was due to FASN activity, we silenced its expression in ECs using lentiviral vectors encoding two non-overlapping FASN-specific short hairpin RNAs (shRNAs) (shFASN) and non-overlapping RNAi oligomers, which lowered FASN levels (Figures S1A–S1F). FASN knockdown (FASN$_{KD}$) or use of the FASN blocker orlistat reduced ^{14}C label incorporation into FAs in ECs (Figures 1A and 1B), similarly as in other cell types (Kridel et al., 2004). Notably, orlistat inhibited FASN in ECs at concentrations 10- to 20-fold lower than those used to inhibit FASN in cancer cells (Yang et al., 2015). When using FA-depleted medium, ECs upregulated FASN protein (Figure S1G) and FA synthesis levels (Figure 1C). We reanalysed in-house transcriptomics data of murine tumor ECs (TECS) versus normal ECs (NECs) (Cantelmo et al., 2016), as well as published transcriptomics studies of murine and human TECs versus NECs (Phoenix et al., 2016; Roudnicky et al., 2013; Wragg et al., 2016). This meta-analysis revealed that FASN was overexpressed in TECs (Figure 1D; p = 1.0 3 10_20). Compared with cancer cells, known to express FASN (Hou et al., 2008; Hunt et al., 2007), ECs had lower FASN protein levels (Figure S1H). Incorporation of ^{14}C label from [U-^{14}C]-glucose into FAs was lower in ECs than in cancer cells, except for MCF7 cells (Figure 1E).

FASN Promotes Vessel Sprouting In Vitro

FASN$_{KD}$ or a low concentration of orlistat (10 mM) decreased EC proliferation (Figures 1F, 1G, and S1I–S1L). As the outcome of EC migration assays is influenced by EC proliferation, we analyzed the migratory behavior of ECs upon mitotic inactivation by mitomycin C (mitoC) (De Bock et al., 2013). FASN$_{KD}$ did not impair migration of mitoC-treated ECs, as measured in the scratch wound assay (Figure 1H) and only minimally reduced EC motility in the Boyden chamber assay (Figure 1I). Analysis of the velocity and directionality of spontaneous migration confirmed that FASN$_{KD}$ did not reduce EC motility (Figures 1J and 1K). Using the EC spheroid model (Schoors et al., 2015), FASN$_{KD}$ or orlistat reduced EC sprouting (Figures 1L–1P and S1M–S1P). MitoC impaired vessel sprouting, but FASN$_{KD}$ was unable to further reduce sprouting upon mitoC treatment, showing that FASN$_{KD}$ impaired vessel sprouting primarily by reducing EC proliferation, not migration (Figures 1N–1P and S1M).

FASN Gene Deletion in ECs Impairs Physiological Angiogenesis In Vivo

To study the in vivo relevance of endothelial FASN deficiency, we crossed FASN$_{lox/lox}$ mice (Wei et al., 2011) with VE-cadherin(PAC)-Cre^{ERT2} mice, a tamoxifen-inducible EC-specific Cre-driver line (Benedito et al., 2009). Treatment of doubletransgenic pups with tamoxifen at postnatal day 1 (P1) to P3 yielded viable FASN$_{DvEC}$ mice, in which FASN was deleted in ECs (Figures S2A and S2B). Staining of retinal vessels with isolectin-B4 (IB4) revealed that EC loss of FASN reduced the number of vascular branch points and total vascular area (Figures 2A–2E). The vascular defects in FASNDvEC mice were due to reduced EC proliferation (Figures 2F–2H), and FASNDvEC mice had a normal number of filopodia per 100-mmvascular front perimeter (Figures 2I–2K). The vascular defect in FASNDvEC mice was not due to vessel regression, as staining for IB4 and collagen IV did not reveal a change in the fraction of empty sleeves (Figures 2L–2N). Vessel maturation was normal in FASNDvEC mice (Figures S2C–S2E). Similar effects were seen in conditional FASNDEC mice when a tamoxifen-inducible platelet-derived growth factor Cre-recombinase line was used as EC-

https://doi.org/10.1016/j.cmet.2018.07.019

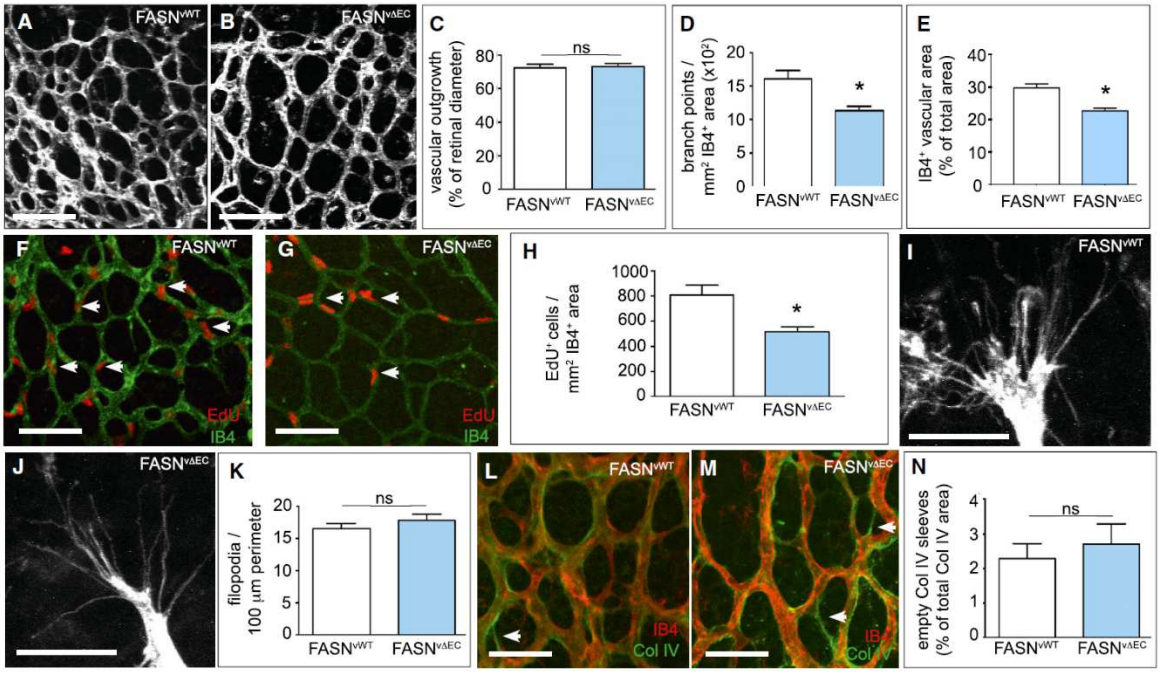

Figure 2. Effect of FASN Gene Deletion in ECs on Physiological Angiogenesis In Vivo

(A and B) Representative confocal images of isolectin-B4 (IB4)-stained retinal vessels of neonatal mice at postnatal day 5 (P5), showing reduced vascular branching upon EC-specific (VE-Cadherin-Cre) deletion of FASN ($FASN_{vDEC}$) (B) as compared with wild-type ($FASN_{vWT}$) (A) pups. Scale bars, 100 mm.

(C) Quantification of retinal vascular outgrowth (radial expansion in percent of retinal diameter) in $FASN_{vWT}$ (n = 17) and $FASN_{vDEC}$ (n = 20) mice.

(D) Number of branch points in the retinal vasculature of $FASN_{vWT}$ (n = 17) and $FASN_{vDEC}$ (n = 20) mice.

(E) $IB4_+$ retinal vascular area (expressed as percent of total area) in $FASN_{vWT}$ (n = 7) and $FASN_{vDEC}$ mice (n = 7).

(F and G) Representative confocal images of the vascular front in the retinal vasculature stained for 5-ethynyl-2o-deoxyuridine (EdU) (red) and isolectin-B4 (IB4) (green) in $FASN_{vWT}$ (F) and $FASN_{vDEC}$ (G) mice. Arrows denote EdU_+ ECs. Scale bars, 100 mm.

(H) Number of proliferating EdU_+ ECs in the retinal vasculature of $FASN_{vWT}$ (n = 9) and $FASN_{vDEC}$ (n = 7) mice.

(I and J) Representative high-magnification confocal images of ECs at the retinal vascular front (isolectin-B4 staining) in $FASN_{vWT}$ (I) and $FASN_{vDEC}$ (J) pups. Scale bars. 25 mm.

(K) Number of filopodia per 100-mm perimeter of the retinal vascular front in $FASN_{vWT}$ (n = 14) and $FASN_{vDEC}$ (n = 16) pups.

(L and M) Representative confocal images of the retinal vasculature stained for isolectin-B4 (red) and the basement membrane marker collagen IV (green) in $FASN_{vWT}$ (L) and $FASN_{vDEC}$ (M) mice. Arrows denote isolectin-$B4_-$ collagen IV_+ empty sleeves (green vascular profiles consisting only of green basement membrane without red ECs). Scale bars, 50 mm.

(N) Percentage of isolectin-$B4_-$ collagen IV_+ empty sleeves compared with the total collagen IV_+ vascular area in $FASN_{vWT}$ (n = 7) and $FASN_{vDEC}$ (n = 9) mice. Data are mean ± SEM. *$p < 0.05$ by standard two-tailed t test; ns, not significant. See also Figure S2.

specific driver line (FASNDpEC) (Figures S2F–S2Q). Thus, impaired angiogenesis in FASNDpEC mice was also due to EC proliferation defects.

Effects of FASN Silencing on EC Metabolism

$FASN_{KD}$ did not affect glycolysis, glucose, or glutamine oxidation (Figures 3A–3C), but reduced FA oxidation (FAO), though by no more than 30% (Figure 3D), consistent with the fact that malonyl-CoA inhibits carnitine palmitoyltransferase 1A (CPT1A, a rate-controlling enzyme of FAO) and malonyl-CoA levels were elevated in $FASN_{KD}$ cells (see below). $FASN_{KD}$ did not affect label incorporation from [U-$_{13}$C]-glucose or [U-$_{13}$C]-glutamine into tricarboxylic acid (TCA) cycle intermediates, but slightly reduced label incorporation from [U-$_{13}$C]-palmitate, in line with the reduced FAO (Figures S3A–S3C). FASN silencing or blockade did not cause energy distress, as determined by measuring the energy charge or p-AMPK levels (Figures 3E, 3F, and S3D). This is not surprising, since FAO contributes only minimally (<5%) to the total ATP production in ECs, which relies primarily on glycolysis (De Bock et al., 2013), and FAO was reduced only moderately. Measurements of cellular reactive oxygen species (ROS) levels in baseline and upon challenge with exogenous H2O2 (Figure 3G), in combination with quantification of oxidized glutathione (GSSG) levels (Figure 3H), revealed that FASNKD did not cause redox imbalance or the ability of ECs to cope with exogenous oxidative stress. Even though FAO supports EC proliferation by providing acetyl-CoA to sustain the TCA cycle for dNTP synthesis in conjunction with an anaplerotic carbon source (Schoors et al., 2015), the modest reduction of FAO in FASNKD cells did not likely explain their proliferation defect (Figures S3E–S3N).

FASN Silencing Moderately Affects Palmitate Levels in ECs

Impairment of proliferation and viability of cancer cells upon inhibition of FASN or acetyl-CoA carboxylase (ACC) has been attributed to depletion of cellular palmitate pools by 50%– 97%, sufficient to cause ER stress and apoptosis (Ventura et al., 2015). $FASN_{KD}$ lowered palmitate levels only by ±20% in ECs (Figure 3I), likely because ECs can take up FAs from the medium or recycle membrane lipids (Rohrig and Schulze, 2016). Import of [U-$_{14}$C]-palmitate was not compensatorily increased by $FASN_{KD}$ (Figure S4A) or orlistat, in contrast to sulfo-N-succinimidyl oleate (SSO), an inhibitor of FA translocase CD36 (Kuda et al., 2013) (Figure S4B), suggesting that the palmitate uptake capacity of ECs is sufficient to maintain cellular palmitate pools. Consistent with reduced de novo palmitate synthesis, the fraction of monounsaturated fatty acyl chains was moderately decreased in $FASN_{KD}$ ECs (Figures S4C and S4D).

https://doi.org/10.1016/j.cmet.2018.07.019

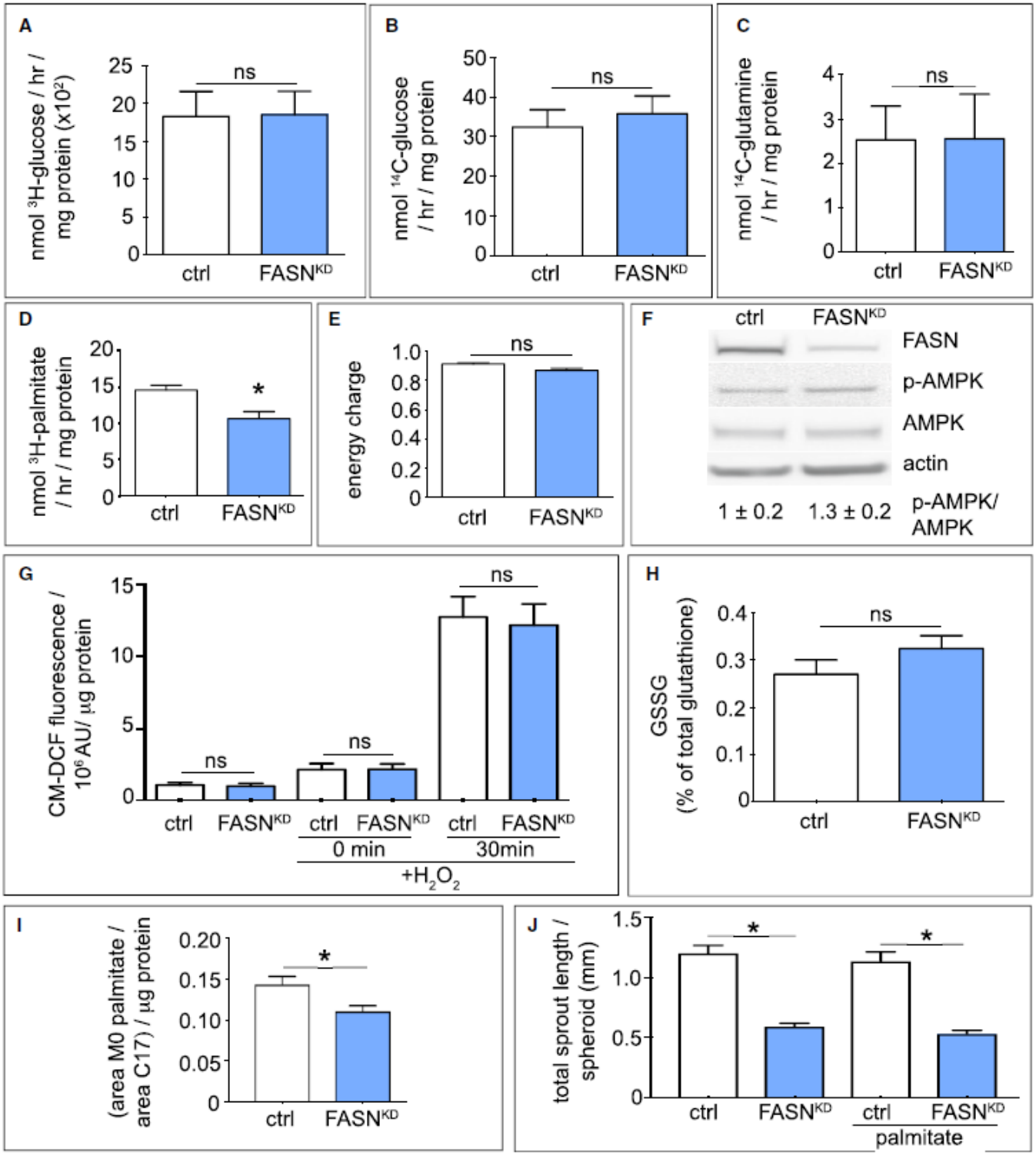

Figure 3. Effect of FASN Silencing on EC Metabolism

(A–D) Effect of FASN silencing (FASN$_{KD}$) in ECs on glycolysis (A), glucose oxidation (B), glutamine oxidation (C), or fatty acid oxidation (D) (A–C: n = 3, D: n = 4).

(E and F) Effect of FASN silencing (FASN$_{KD}$) in ECs on energy charge (([ATP] + 1/2 [ADP])/([ATP] + [ADP] + [AMP])) (E), and on AMPK phosphorylation as verified by immunoblotting (F) (n = 3). Actin was used as loading control in (F). Densitometric quantification of the p-AMPK/AMPK ratio, expressed relative to control, is shown beneath the blot.

(G) Intracellular ROS levels (CM-DCF fluorescence) in control and FASN$_{KD}$ ECs in baseline and upon supplementation with 50 mM H_2O_2 for 30 min (n = 3). AU, arbitrary units.

(H) Oxidized glutathione levels (percent of GSH + GSSG) in control and FASN$_{KD}$ ECs (n = 3).

(I) Quantification of intracellular palmitate levels (normalized to the standard C17 peak area) in control and FASN$_{KD}$ ECs (n = 3).

(J) Quantification of total sprout length of control (ctrl) and FASN$_{KD}$ spheroids grown in medium without or with supplementation with palmitate (50 mM) (n = 3). Data are mean ± SEM. *$p < 0.05$ by standard two-tailed t test with Welch's correction (A–F and H–I) or ANOVA (G and J); ns, not significant. See also Figures S3 and S4.

https://doi.org/10.1016/j.cmet.2018.07.019

The reduced pool of palmitate in FASN$_{KD}$ ECs was insufficient to cause ER stress and cell death (Figures S4E–S4I and S5A). Unlike cancer cells (Svensson et al., 2016), supplementation of palmitate, elevating cellular palmitate pools in FASN$_{KD}$ ECs even slightly above the levels in control cells (Figure S5B), did not rescue the FASN$_{KD}$ sprouting defect (Figure 3J). Thus, the sprouting defect of FASN$_{KD}$ ECs was not due to the depletion of cellular palmitate pools.

FASN Silencing Increases Malonyl-CoA Levels

We then explored whether FASN$_{KD}$ enhanced the accumulation of its substrate malonyl-CoA. Lipogenesis involves conversion of acetyl-CoA to malonyl-CoA by ACC, and the use of malonyl-CoA and acetyl-CoA by FASN to synthesize palmitate. FASN$_{KD}$ or orlistat substantially elevated malonyl-CoA levels, without affecting acetyl-CoA levels (Figures 4A, 4B, and S5C). To explore whether the elevated malonyl-CoA levels contributed to the sprouting defects, we silenced the expression of acetyl-CoA carboxylase 1 (ACC1), which is expressed more abundantly than its isoenzyme ACC2 in ECs (Figure S5D). ACC1 knockdown (ACC1$_{KD}$; lowering ACC1 mRNA levels by 83%) alone did not affect malonyl-CoA levels, but when both FASN and ACC1 were silenced, malonyl-CoA levels were no longer increased (Figure 4C). Silencing of malonyl-CoA decarboxylase (catalysing the reverse reaction of ACC1) and of SIRT5 (a de-malonylase [Nishida et al., 2015]) did not induce changes in protein malonylation in ECs (not shown). ACC1$_{KD}$ alone reduced vessel sprouting and EC proliferation (Figures 4D, 4F, 4H, and 4I) (a more prominent anti-mitogenic effect was reported for cancer cells [Svensson et al., 2016]). More importantly, however, when both FASN and ACC1 were silenced together, EC proliferation and vessel sprouting were similar relative to ACC1$_{KD}$ cells, showing that the anti-proliferative effect of FASN$_{KD}$ was abrogated by ACC1$_{KD}$ (Figures 4D–4I and S5E). Thus, FASN$_{KD}$ impaired sprouting and EC proliferation partly by elevating malonyl-CoA levels.

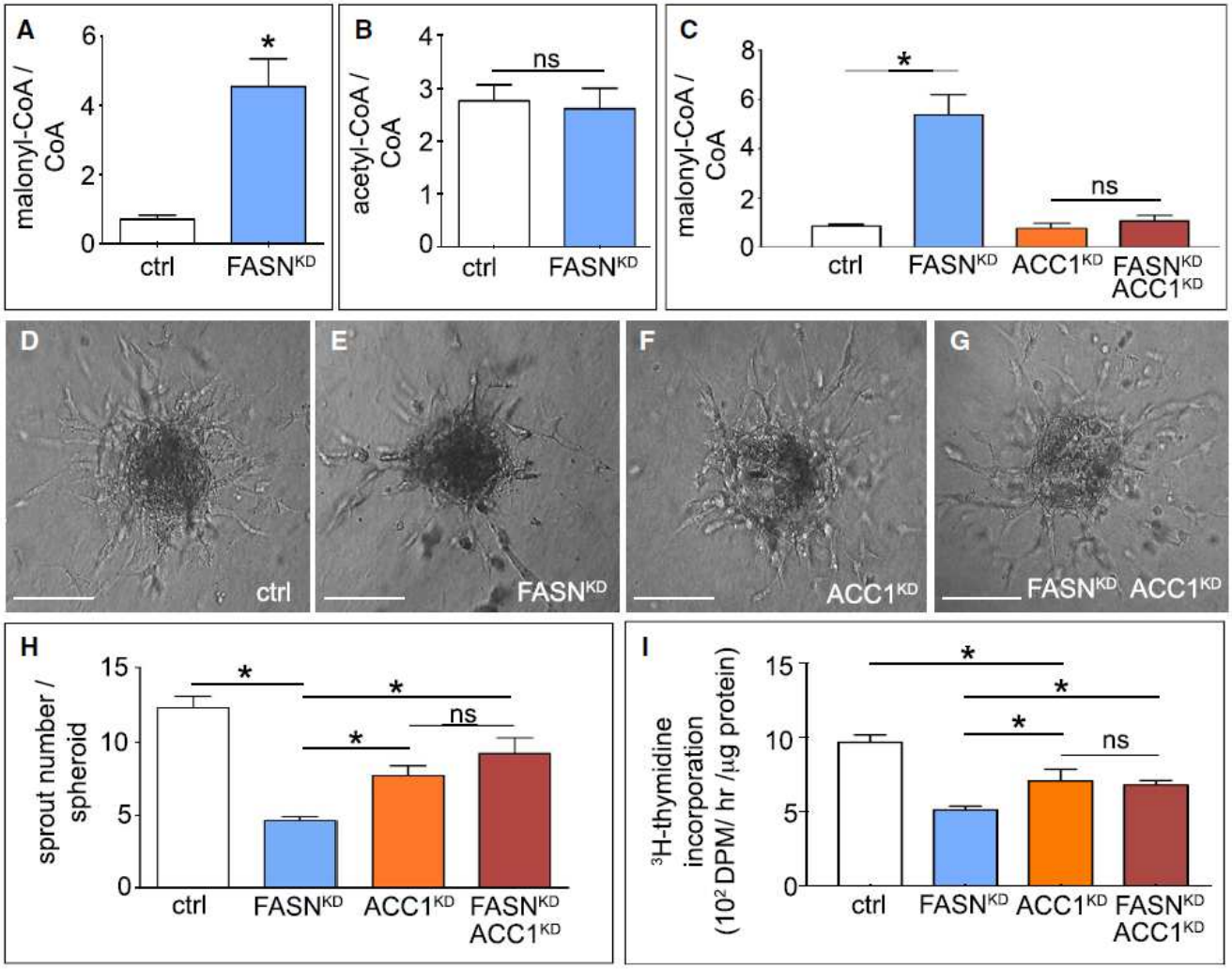

Figure 4. Effect of FASN Silencing on Malonyl-CoA Levels

(A) Malonyl-CoA/CoA ratio in control and FASN$_{KD}$ ECs (n = 4).

(B) Acetyl-CoA/CoA ratio in control and FASN$_{KD}$ ECs (n = 4).

(C) Malonyl-CoA/CoA levels in ECs upon single or combined knockdown of ACC1 (ACC1$_{KD}$) and FASN (FASN$_{KD}$) (n = 3).

(D–G) Representative phase-contrast images of EC spheroids using control ECs (D) or ECs with single (E and F) or combined (G) silencing of ACC1 (ACC1$_{KD}$) and FASN (FASN$_{KD}$). Scale bars, 150 mm.

(H) Sprout number of EC spheroids as in (D) to (G) (n = 4).

(I) [^{3}H]-Thymidine incorporation into DNA (proliferation assay) in control ECs and ECs with single or combined knockdown of ACC1 (ACC1$_{KD}$) and FASN (FASN$_{KD}$) (n = 4). DPM, disintegrations per minute. Data are mean ± SEM. *p < 0.05 by ANOVA (C, H, and I) or standard two-tailed t test with Welch's correction (A and B); ns, not significant. See also Figures S4 and S5.

https://doi.org/10.1016/j.cmet.2018.07.019

FASN Silencing Induces Malonylation of mTOR

We explored whether the increased malonyl-CoA levels influenced protein malonylation, a poorly studied non-enzymatic PTM driven by substrate levels (Peng et al., 2011). Immunoblotting of lysates for malonylated lysine residues (Kmal) revealed that $FASN_{KD}$ or orlistat elevated general Kmal levels in ECs (Figures 5A and S5F). To identify malonylated proteins, we performed a proteomics screen using an anti-Kmal antibody to enrich Kmal peptides and analyzed Kmal peptides as reported by Colak et al. (2015). We identified nearly 100 Kmal sites in 64 different proteins, of which 62 were reported in other malonylome screens, validating our approach (Table S1). Among the proteins with Kmal sites, we identified targets involved in pathways previously shown to be modified by lysine malonylation, including glycolysis, pentose phosphate pathway, and cytoskeleton remodeling (Table S1) (Nishida et al., 2015).

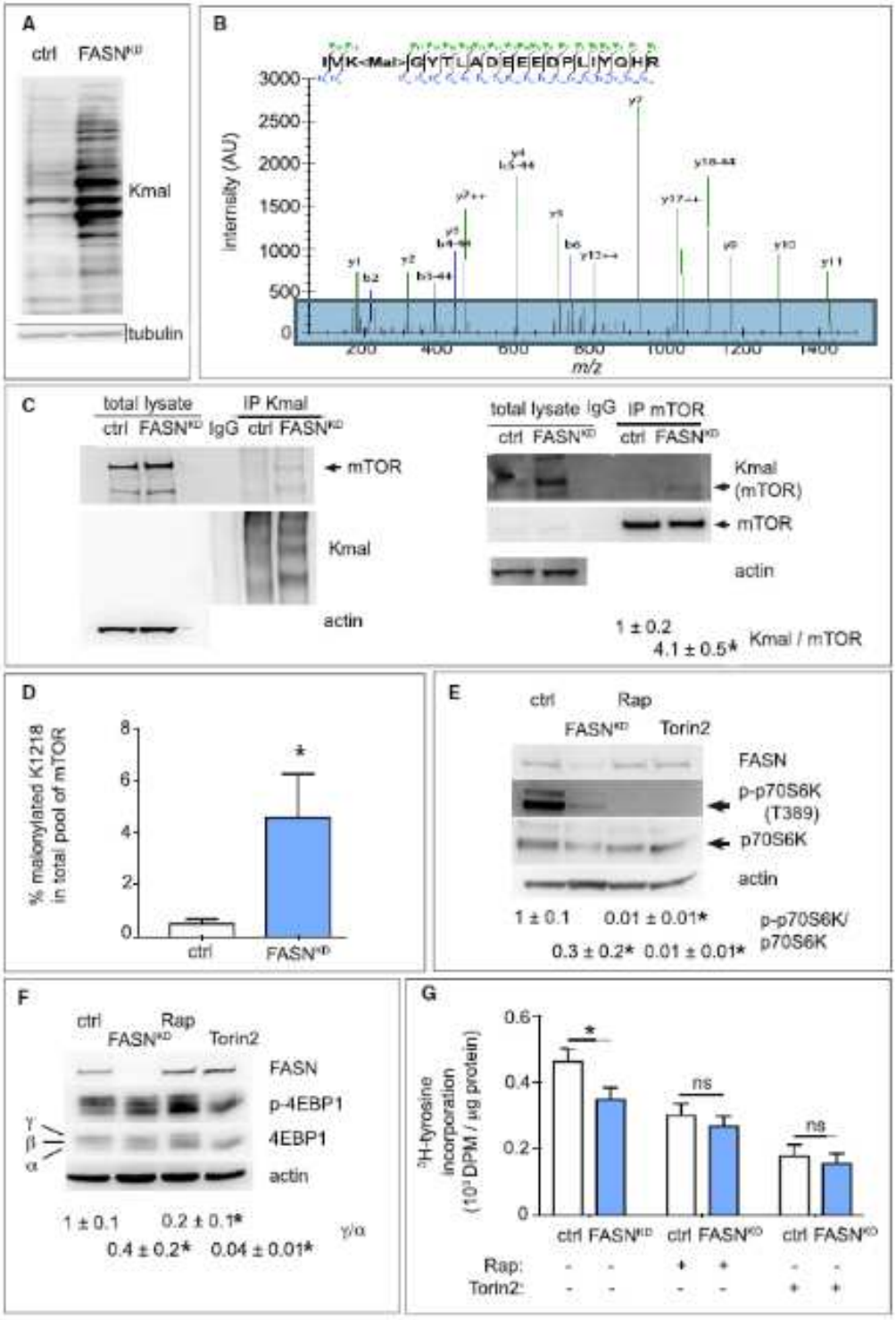

Figure 5. Effect of FASN Silencing on mTOR Malonylation and Activity

(A) Representative immunoblot of lysine malonylated (Kmal) proteins in control and $FASN_{KD}$ ECs. Tubulin was used as loading control.

(B)MS/MS validation of themTOR K1218malonylation site. The fragmentation spectrumof the trypticmTOR peptideH_2N_{1216}IVK<mal>GYTLADEEEDPLIYQHR$_{1235}$-COOH(825.7395m/z, 3+) carrying themodification is shownwith annotated y-ions (green) and b-ions (blue). The b-ion series covers themalonylation site and displays the typical neutral loss of 44 Da (corresponding to the loss of CO_2).

https://doi.org/10.1016/j.cmet.2018.07.019

(C) Representative western blots of immunoprecipitated (IP) endogenous malonylated proteins (Kmal; left blot) or mTOR (right blot) and immunoblotted for the reciprocal proteins in control and $FASN_{KD}$ ECs. Actin was used as loading control. Arrowheads indicate malonylated (Kmal) or total mTOR band. Densitometric analysis of the Kmal mTOR to total mTOR ratio, expressed relative to control, is shown beneath the blots (n = 3).
(D) Stoichiometry of mTOR-K1218 malonylation determined by novel LC-MS/MS methods, in control and $FASN_{KD}$ ECs (n = 4).
(E) Representative immunoblot of total (p70S6K) and phosphorylated (p-p70S6K threonine 389 [T389]) p70S6K in control (ctrl) and $FASN_{KD}$ ECs. Actin was used as loading control. The mTORC1 inhibitor rapamycin (Rap) (20 nM) and mTORC1/2 inhibitor Torin2 (100 nM) were used as positive controls. Densitometric quantification of the p-p70S6K/p70S6K ratio, expressed relative to ctrl, is shown beneath the blots (n = 3).
(F) Representative immunoblot of total 4EBP1 and phosphorylated p-4EBP1 in control and $FASN_{KD}$ ECs. Actin was used as loading control (ctrl). The mTORC1 inhibitor rapamycin (Rap) (20 nM) and mTORC1/2 inhibitor Torin2 (100 nM) were used as positive controls. Densitometric analysis of the ratio between the high phosphorylated g over low phosphorylated a form of p-4EBP1, expressed relative to ctrl, is shown beneath the blots (n = 3).
(G) [^{3}H]-Tyrosine incorporation (protein synthesis) in control (ctrl) and $FASN_{KD}$ ECs, treated with control vehicle, or 20 nM rapamycin (Rap) or 100 nM Torin2 (n = 4). DPM, disintegrations per minute. Data are mean ± SEM. *$p < 0.05$ by ANOVA (G) or standard two-tailed t test with Welch's correction (C–F); ns, not significant. See also Figures S5 and S6; Tables S1 and S2.

Among the identified Kmal proteins, we focused on the mechanistic target of rapamycin (mTOR), a serine/threonine kinase activated by anabolic signals (Saxton and Sabatini, 2017), as it controls lipid synthesis, cell growth, metabolism, and other cell processes in response to nutrition (Saxton and Sabatini, 2017). A report that mTOR complex 1 (mTORC1) blockade by rapamycin inhibits ocular angiogenesis (Yagasaki et al., 2014b) primed our interest to focus on this target. The mTOR kinase nucleates two protein complexes named mTORC1 and mTORC2. The proteomic analysis identified only one malonylated lysine residue in mTOR (K1218), showing a characteristic tandem mass spectrometry (MS/MS) spectrum including C-terminal y-ions and amino-terminal b-ions (Table S1 and Figure 5B).

Immunoprecipitation of endogenous mTOR followed by immunoblotting for Kmal (also in the reverse order for $FASN_{KD}$ cells) confirmed that mTOR was malonylated, and that malonylated mTOR levels were increased in $FASN_{KD}$ or orlistat-treated ECs (Figures 5C and S5G). The weak immunoblot signals are attributable to the fact that only one lysine is malonylated in mTOR and, possibly, that only a fraction of the endogenous mTOR pool in ECs is malonylated. Indeed, when generating a tryptic peptide containing a stably malonylated K1218 of mTOR to measure the malonylation stoichiometry via MS, we found 4.5% of the mTOR pool to be malonylated in $FASN_{KD}$ ECs (Figure 5D).

Malonylation of mTOR Reduces mTORC1 Activity

To assess whether mTOR malonylation affected the activity of its complexes, we analyzed phosphorylation of the downstream targets of mTORC1 (eukaryotic translation initiation factor 4Ebinding protein 1 [4EBP1]; p70 S6 kinase [p70S6K]) and mTORC2 (Akt), using the mTORC1 inhibitor rapamycin and the mTORC1/mTORC2 inhibitor torin2 as positive controls (Saxton and Sabatini, 2017). $FASN_{KD}$ (inducing mTOR malonylation) reduced mTORC1's activity to phosphorylate p70S6K and 4EBP1 (Figures 5E and 5F). In line with reports that 4EBP and p70S6K regulate protein synthesis downstream of mTORC1 (Saxton and Sabatini, 2017), de novo protein synthesis was reduced upon $FASN_{KD}$ (Figure 5G). Treatment of control cells with rapamycin or torin2 reduced protein synthesis, which could not be further decreased by $FASN_{KD}$ (Figure 5G). In agreement with findings that p70S6K regulates cell size (Saxton and Sabatini, 2017), $FASN_{KD}$ reduced EC size (Figure S5H).

In contrast, $FASN_{KD}$ lowered phosphorylation of mTORC2's target Akt (Figure S6A), but less prominently than of mTORC1 targets, and not consistently across different assays (see below). Possibly, the effect by $FASN_{KD}$ on p-Akt relates to the reduced confluence of these cells (cell-cell contacts activate Akt [Taddei et al., 2008]). Though not extensively documented, certain PTMs of mTOR correlate with changes in the activity of mTORC1, not of mTORC2 (Rosner et al., 2010). While remaining unexplained, the more selective regulation of mTORC1, rather than mTORC2, pathway activity by mTOR malonylation may thus not be surprising. Additional $ACC1_{KD}$ in $FASN_{KD}$ ECs normalized the malonylated mTOR levels to those in control cells and restored mTORC1's activity (Figures S6B–S6D); FASN overexpression yielded similar results (Figures S6E and S6F).

Malonylation of mTOR upon $FASN_{KD}$ reduced the enzymatic activity of mTORC1, in two complementary assays (radioactive phosphor donor [Dunlop et al., 2009]; commercial ELISA-based kit) (Figures 6A and 6B), without, however, affecting its stability or intracellular localization (Figures S6G, S6H, and S7A). FASN inhibition by orlistat yielded largely similar results (Figure 6B), although phosphorylation of Akt was unchanged (see below). We also assessed whether mTOR malonylation decreased mTORC1's activity independently of FASN inhibition by employing malonyl-NAC (N-acetylcysteamine), a cell-permeable agent capable of directly inducing cellular protein malonylation (Kulkarni et al., 2017). Similar to $FASN_{KD}$ cells, malonyl-NAC treatment of control ECs reduced mTORC1's activity (Figure 6B) and target phosphorylation (Figure 6C), illustrating that direct malonylation of mTOR, independently of FASN manipulation, sufficed to reduce mTORC1's activity.

mTOR Mutagenesis Studies

To test whether the increased mTOR malonylation contributed to the vascular defects upon FASN inhibition, we mutated K1218 of mTOR into glutamic acid (E) in order to mimic constitutive malonylation ($mTOR_{K/E}$) (Nishida et al., 2015). To avoid any confounding interpretation resulting from endogenous wild-type (WT) mTOR expression, we silenced mTOR (lowering mRNA levels by 60%–70%; Figure S7B) and expressed wild-type mTOR ($mTOR_{WT}$) or $mTOR_{K/E}$, both resistant to the mTOR-specific shRNA (Figure S7B). To avoid additional stress for ECs resulting from multiple viral transductions, we used orlistat to inhibit FASN. Compared with $mTOR_{WT}$, $mTOR_{K/E}$ expression reduced protein synthesis in control cells to similar levels as in orlistat-treated $mTOR_{WT}$ cells, while protein synthesis was not further reduced by orlistat in $mTOR_{K/E}$ cells (Figure 6D).
Similar results were obtained when analyzing phosphorylation of p70S6K and 4EBP1 (Figure 6E) and vessel sprouting (Figures 6F–6M and S7C). Also, $mTOR_{K/E}$ reduced mTORC1's enzymatic activity to levels similar to those of $FASN_{KD}$ or orlistat (Figure 6B).

https://doi.org/10.1016/j.cmet.2018.07.019

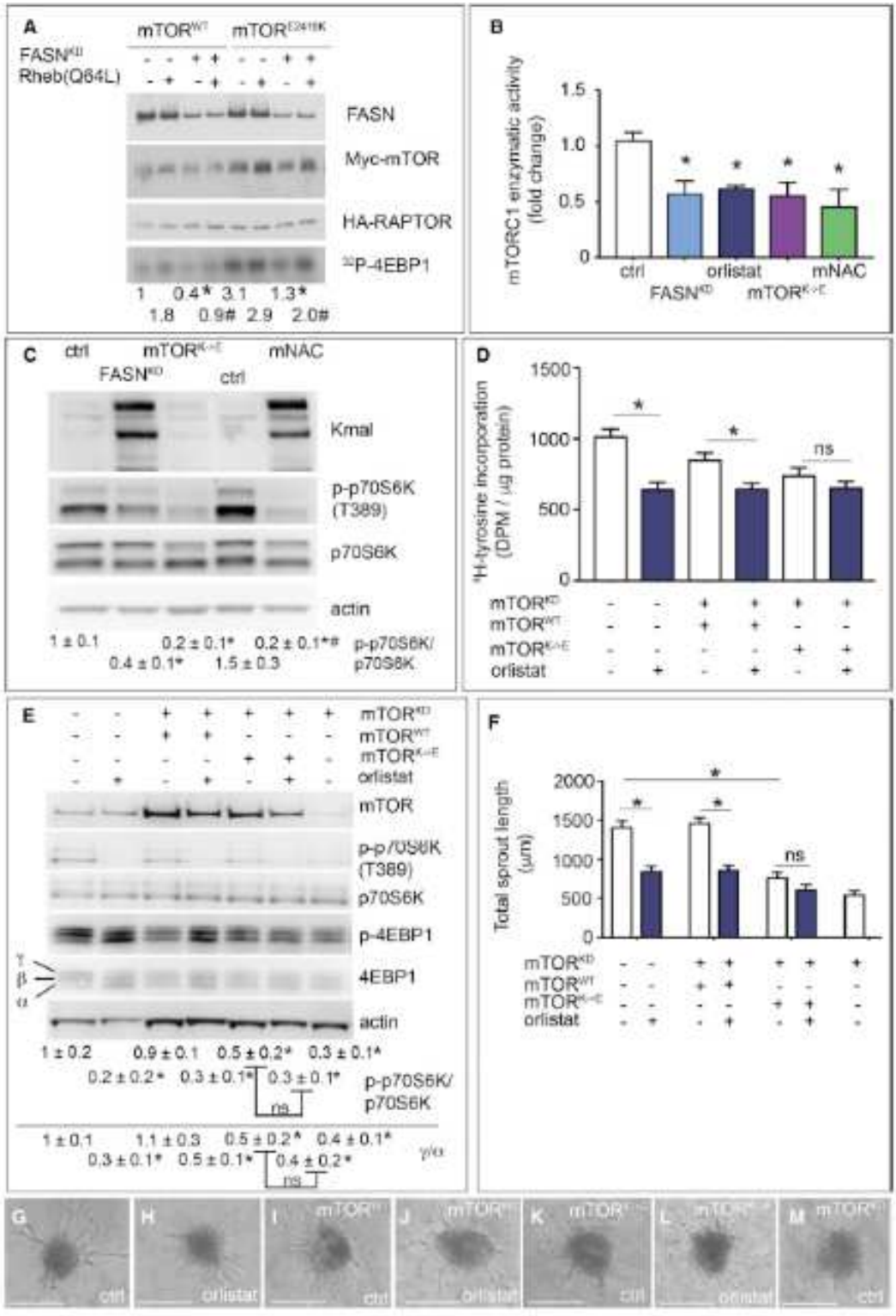

Figure 6. Role of Lysine 1218 in the Regulation of mTORC1 Activity upon FASN Blockade

(A) Enzymatic mTORC1 kinase assay measuring phosphorylation of recombinant 4EBP1 ([32P]-4EBP1) in HEK293T cells overexpressing myc-mTOR and HA-RAPTOR. Top: immunoblotting for FASN of total lysates of control or FASN-silenced ($FASN_{KD}$) HEK293T cells overexpressing either myc-tagged wild-type mTOR ($mTOR_{WT}$) (first 4 columns) or a myc-tagged highly active E2419K mutant of mTOR (last 4 columns), with or without addition in the kinase reaction mixture of recombinant Rheb Q64L, a highly active mutant of the mTORC1 activator Rheb. Middle (rows 2 and 3): immunoblotting for myc-mTOR (row 2) or HA-RAPTOR (row 3) of lysates of the above listed cells after immunoprecipitation of the mTORC1 complex using anti-myc antibodies. Immunoblotting for myc-mTOR is shown to confirm mTOR overexpression; immunoblotting for HA-raptor is shown as loading control for the kinase assay. Bottom: representative autoradiograms of [32P]-4EBP1. Densitometric quantification of the [32P]-4EBP1 bands, expressed as fold change relative to control (column 1) is shown beneath the autoradiogram. The more active E2419K mutant of mTOR was overexpressed to enhance the AR signal (last 4 lanes).

https://doi.org/10.1016/j.cmet.2018.07.019

(B) mTORC1 enzymatic activity (K-LISA mTOR activity kit [Millipore]) in control (ctrl), FASN-silenced ($FASN_{KD}$), orlistat-treated ECs, ECs expressing mTOR harboring a K1218E mutation ($mTOR_{K/E}$, malonylation mimicking), and ECs treated with malonyl-NAC (mNAC, a cell-permeable malonyl-CoA mimic) (n = 3). Values were normalized to protein input and are expressed as fold change relative to control.
(C) Representative immunoblot of Kmal, total and phosphorylated p70S6K, and actin as loading control, in control (ctrl) and FASN-silenced ($FASN_{KD}$) ECs, ECs expressing mTOR harboring a K1218E mutation ($mTOR_{K/E}$, malonylation mimicking), and ECs treated with malonyl-NAC (mNAC, a cell-permeable malonyl-CoA mimic). Densitometric quantification of the p-p70S6K/p70S6K ratio, expressed relative to control, is shown beneath the blot (n = 3).
(D) [3H]-Tyrosine incorporation in control and orlistat (10 mM)-treated ECs, silenced for endogenous mTOR ($mTOR_{KD}$) as indicated and expressing a wild-type mTOR ($mTOR_{WT}$) or mTOR harboring a K1218E ($mTOR_{K/E}$) mutation (both resistant to the mTOR shRNA) (n = 4). DPM, disintegrations per minute.
(E) Representative immunoblot of total and phosphorylated levels of the mTORC1 targets p70S6K and 4EBP1 in control ECs and ECs silenced for endogenous mTOR ($mTOR_{KD}$) with or without overexpression of wild-type mTOR ($mTOR_{WT}$) or mTOR harboring a K1218E ($mTOR_{K/E}$) mutation (both resistant to the mTOR shRNA) and with or without FASN inhibition (orlistat). Densitometric quantification of the p-p70S6K/p70S6K ratio or of the ratio between the high phosphorylated g over low phosphorylated a form of 4EBP1 (expressed relative to ctrl ECs) is shown beneath the blots (n = 3).
(F) Quantification of vessel sprouting from spheroids shown in (G) to (M) (n = 3).
(G–M) Representative phase-contrast images of control (ctrl) and orlistat-treated EC spheroids using wild-type ECs (G and H), or ECs silenced for endogenous
mTOR ($mTOR_{KD}$) and expressing mTOR WT ($mTOR_{WT}$) (I and J) or mTOR K1218 mutant ($mTOR_{K/E}$) (both resistant to the mTOR shRNA) (K and L). (M) shows a representative spheroid using $mTOR_{KD}$ ECs. Scale bars, 200 mm.
Data are mean ± SEM. In (A), *p < 0.05, #p < 0.05 for $FASN_{KD}$ versus its corresponding FASN wild-type in each condition. In (B), (D), and (F), *p < 0.05 by ANOVA. In
(E), *p < 0.05 for orlistat versus its corresponding control, or for $mTOR_{KD}$ versus control (column 1), by standard two-tailed t test with Welch's correction. In (C),
*p < 0.05 versus its respective control and #p < 0.05 for mNAC versus $FASN_{KD}$, determined by ANOVA followed by t test. ns, not significant. See also Figure S7.

To confirm specificity, we mutated mTOR K1218 into arginine ($mTOR_{K/R}$) in order to prevent malonylation, an approach widely used in the acetylation field (Baeza et al., 2016), though never performed in the malonylation field to date (in higher eukaryotes). Overexpression of $mTOR_{WT}$ in control cells (in which endogenous mTOR expression was not silenced) elevated mTOR malonylation upon $FASN_{KD}$ (Figure S7D). In contrast, overexpression of $mTOR_{K/R}$ in control cells elevated mTOR malonylation much less upon $FASN_{KD}$ (Figure S7D), the residual increase resulting from endogenous WT mTOR. Using a similar strategy as employed for $mTOR_{K/E}$, we observed that $mTOR_{K/R}$ abrogated the decrease of p-p70S6K/p70S6K levels upon $FASN_{KD}$ (Figure S7E). When analyzing vessel sprouting, overexpression of $mTOR_{K/R}$ in control cells induced a small baseline effect (consistent with reports of $mTOR_{K/R}$ in other assays [Gorsky et al., 2016]), but abrogated the decrease upon $FASN_{KD}$ as observed in $mTOR_{WT}$-expressing cells (Figure S7F). As mentioned, orlistat did not reduce p-Akt/Akt levels in control ECs or ECs re expressing $mTOR_{WT}$, $mTOR_{K/E}$, or $mTOR_{K/R}$ (Figure S7G).

Pharmacological FASN Blockade Reduces Angiogenesis and Vascular Defects

Pharmacological compounds blocking FASN (orlistat) are being used to treat obesity (Point et al., 2016). However, in preclinical models, orlistat induces weight loss when used at a very high dose (240 mg/kg/day) (Kridel et al., 2004). We therefore used orlistat at a low dose (10 mg/kg/day) that did not cause body weight loss (Figure 7A). Treatment of pups with orlistat from P1 to P4 caused qualitatively similar vascular changes as observed in $FASN_{DEC}$ mice, including reduced vessel branching and EC proliferation, without affecting EC migration (Figures 7B–7G).
To test the therapeutic potential of FASN blockade in pathological angiogenesis, we used the model of retinopathy of prematurity (ROP), since the vascular tufts induced by ischemia primarily consist of proliferating ECs (Schoors et al., 2015). Treatment of pups with a low dose of orlistat during the vascular proliferation phase reduced vascular tuft formation (Figures 7H– 7J). Immunostaining revealed reduced phosphorylated S6 immunoreactive levels in vascular tufts in orlistat-treated mice similar to rapamycin-treated mice (Figures 7K–7O). Additional staining experiments confirmed reduced levels of phosphorylated p70S6K and unchanged levels of phosphorylated Akt in ECs freshly isolated from $FASN_{vDEC}$ mice, and in pulmonary ECs on fixed lung from $FASN_{vDEC}$ mice (Figures S7H–S7L). Thus, FASN blockade with a low dose of orlistat can inhibit pathological ocular neovascularization by reducing mTOR activity.

DISCUSSION

In addition to mediating de novo lipid synthesis, FASN in ECs indirectly controls PTM of target proteins via lysine malonylation, in particular mTOR, a prime regulator of metabolism. mTOR malonylation upon FASN inhibition reduced mTORC1's enzymatic activity, contributing to vascular defects. Identification of mTOR K1218 Malonylation Using an unbiased proteomic approach in $FASN_{KD}$ ECs, along with complementary biochemical validation, we established that mTOR is malonylated at K1218, embedded in the ICRIVKGYTLA amino acid sequence, containing amino acids (K, R, G, A, V, Y, I) that are often enriched in a lysine malonylation consensus site (Nishida et al., 2015). K1218 in mTOR is acetylated in cancer cells (Choudhary et al., 2009). Since acetylation and malonylation modify lysine residues (Nishida et al., 2015), this finding raises the question of whether mTOR K1218 may be a key node for mTORC1 activity regulation by metabolite second messengers such as malonyl-CoA and acetyl-CoA (Pietrocola et al., 2015). Notably, K1218 in mTOR is conserved in Homo sapiens, Mus musculus, and multiple other species (Table S2). Nonetheless, we acknowledge that increased malonylation of other targets upon FASN inhibition may contribute to the impaired neovascularization. Stoichiometry of mTOR K1218 Malonylation Quantification of the absolute levels of stoichiometry of protein malonylation has never been successfully achieved, due to spontaneous decarboxylation of the malonyl moiety on standard peptides. To date, only one study reported an indirect estimate of malonylation stoichiometry using SILAC ratios (Colak et al., 2015). We developed a targeted liquid chromatography-MS assay for quantification of absolute levels of malonylated versus total mTOR, employing a malonylated stable isotope labelled reference peptide (synthesized with Fmoc-Lys(mono-tert-butylmalonate)-OH as stable precursor for incorporation of the malonylated

https://doi.org/10.1016/j.cmet.2018.07.019

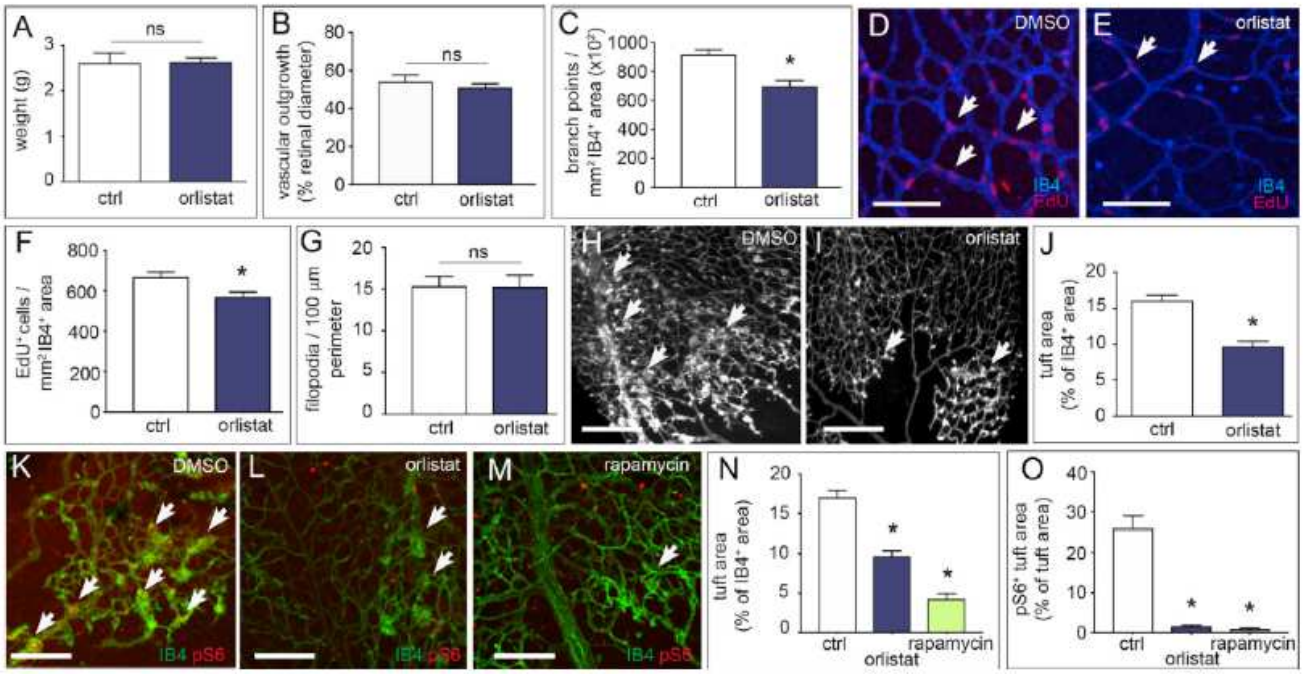

Figure 7. Effect of FASN Blockade on Physiological and Pathological Angiogenesis In Vivo
(A) Body weights of DMSO-treated (ctrl; n = 5) and orlistat-treated (10 mg/kg/day; n = 8) pups at P5.
(B) Quantification of retinal vascular outgrowth (radial expansion in percent of retinal diameter) in pups treated with vehicle DMSO (ctrl; n = 5) or orlistat (n = 8).
(C) Number of branch points in the retinal vasculature of pups treated with vehicle DMSO (ctrl; n = 5) or orlistat (n = 7).
(D and E) Representative confocal images of isolectin-B4 (IB4, blue) and EdU (red) stained retinal vessels at P5 in DMSO-treated (D) and orlistat-treated (E) pups to visualize branching and $IB4_+$ EdU_+ ECs (arrows). Scale bars, 100 mm.
(F) Number of $IB4_+$ EdU_+ ECs per mm_2 of the retinal vasculature of pups treated with vehicle DMSO (n = 5) or orlistat (n = 8).
(G) Number of filopodia per 100 mm perimeter retinal vascular front in vehicle DMSO-treated (ctrl; n = 5) and orlistat-treated (n = 8) pups.
(H and I) Representative images of retinal flat mounts of retinopathy of prematurity (ROP) mice treated with vehicle DMSO (H) or orlistat (I). Arrows denote vascular tufts. Scale bars, 250 mm.
(J) Quantification of vascular tufts in ROP mice treated with vehicle DMSO (ctrl; n = 5) or orlistat (n = 6).
(K–M) Representative confocal images of pS6 and isolectin-B4 (IB4) staining of retinas from ROP mice treated with vehicle (DMSO), orlistat (10 mg/kg/day), or rapamycin (10 mg/kg/day) as positive control. Arrows denote hyperproliferative tufts. Scale bars, 200 mm (n = 4).
(N) Quantification of vascular tufts in ROP mice treated with vehicle (DMSO; ctrl), orlistat, or rapamycin (n = 4).
(O) $pS6_+$ area in vascular tufts in ROP mice treated with vehicle (DMSO; ctrl), orlistat, or rapamycin (n = 4).
Data are mean ± SEM. *$p < 0.05$ by standard two-tailed t test with Welch's correction; ns, not significant.

lysine) and five additional non-modified mTOR peptides as internal standards. Using this assay (useful for future malonylation stoichiometry studies), we reliably quantified the absolute malonylation stoichiometry. This analysis showed mTOR malonylation levels of 4.5% upon $FASN_{KD}$.

These stoichiometry levels may appear low at first sight, but they are nonetheless consistent with reports for other PTMs, in particular acetylation. Indeed, most acetylation sites have very low stoichiometry, not higher than 0.5% (Weinert et al., 2015). An acetylation stoichiometry of 1% is already considered "high," with only five out of thousands of sites having a stoichiometry >5%, and only two sites with a stoichiometry of >10% (Weinert et al., 2015). Studies in other organisms confirmed these data (Meyer et al., 2016). Malonylation cannot be compared with phosphorylation as PTM, as the latter can occur at a much higher stoichiometry, especially during the cell cycle (80%–90% [Olsen et al., 2010]), although the stoichiometry of phosphorylation in response to other stimuli is at most 25% (Sharma et al., 2014). Though not fully appreciated, subpools of a single protein can participate in different biological processes. To induce a biologically relevant effect, PTMs thus may only need to affect the active fraction, not the total protein pool (Baeza et al., 2016). This active fraction might be much smaller than the total pool. Future work will be required to resolve these outstanding questions.

Functional Validation of mTOR K1218 Malonylation, Independent of FASN Inhibition

Protein lysine malonylation was only recently discovered (2011); by transferring a bulky, negatively charged acyl group to a lysine residue, malonylation has been proposed to alter the structure and function of the target protein (Nishida et al., 2015). Indeed, we observed a reduction in mTORC1 pathway activation and, in particular, of mTORC1's enzymatic activity, as determined by two independent cell-free assays.

Site-specific mutagenesis of K1218 showed that malonylation of this residue regulates mTORC1 pathway activation and mTORC1's enzymatic activity, as well as vascular responses. In addition, use of malonyl-NAC revealed that direct malonylation of mTOR, independently of FASN inhibition, was sufficient to induce similar results. All this is consistent with a model whereby inhibition of mTORC1's activity upon FASN silencing or blockade is not an indirect epiphenomenon of FASN inhibition, but a direct effect of mTOR malonylation. The findings also suggest that a partial stoichiometry of mTOR malonylation may suffice and a high stoichiometry of mTOR malonylation is not required to

induce a biological effect (reduced mTORC1 activity). Regardless, to the best of our knowledge, no previous report in the malonylation field determined both the stoichiometry and the functional importance of a malonylation site through mutagenesis and functional validation.

Possible Translational Implications

Treatment with orlistat, the most widely used drug for obesity treatment (Point et al., 2016), reduced ocular neovascularization. The more prominent angiogenesis inhibition in pathological than physiological settings may relate to the fact that ECs more actively proliferate in disease. Increased mTOR and S6 activity levels have been documented in retinal ECs in the ROP model, while mTORC1 blockade reduces ocular angiogenesis (Yagasaki et al., 2014a). In agreement with our model, we observed a decrease of phosphorylated S6 levels in orlistat- treated ROP lesions. A more specific FASN blocker confirmed the orlistat results in the experiments tested (not shown). Confirming our earlier reports (De Bock et al., 2013; Huang et al., 2017; Schoors et al., 2015), emerging evidence shows that EC metabolism differs from that of cancer and immune cells. First, orlistat induces anti-angiogenic effects at >10-fold lower doses than needed to impair tumor growth, offering opportunities to reconsider the use of specific FASN inhibitors as antiangiogenic agent in cancer patients. Second, in cancer cells, orlistat caused cell death by inhibiting mTORC1 (Yang et al., 2015), although in most studies the underlying molecular mechanism was not revealed. Our data identified a mechanism of FASN-dependent regulation of mTOR signaling. Third, ECs differ from cancer cells, in which FASN inhibition depletes the cellular palmitate content (Ventura et al., 2015). These EC-specific properties warrant consideration of FASN as an attractive target to inhibit pathological angiogenesis.

Limitations of the Study

While our study highlights that a low mTOR malonylation stoichiometry suffices to affect mTORC1's enzymatic activity, the precise molecular details of this phenomenon remain to be unveiled.

Our data do not exclude that increased malonylation of other proteins upon FASN inhibition may be involved in the impaired angiogenic response. Nevertheless, the data obtained using ECs expressing $mTOR^{K/E}$ and $mTOR^{K/R}$ mutants, in which malonylation of other proteins was not affected, support a role of mTOR signaling in the angiogenesis phenotype. Furthermore, it would also be insightful to evaluate more specific inhibitors of FASN, once available, for preclinical testing. In conclusion, we discovered a role and therapeutic potential of targeting FASN for pathological neovascularization.

STAR+METHODS

Detailed methods are provided in the online version of this paper

SUPPLEMENTAL INFORMATION

Supplemental Information includes seven figures and two tables and can be found with this article online at https://doi.org/10.1016/j.cmet.2018.07.019.

ACKNOWLEDGMENTS

We acknowledge the help with the lipidomics of Etienne Waelkens. We thank Ralph Adams for providing the VE-cadherin(PAC)-Cre^{ERT2} mice. We thank John Blenis for constructive discussions. U.B. was an FWO fellow and Marie Curie-IEF fellow. K.C.S.Q. was funded by CAPES foundation, Brazil. F.M.-R., J.K., J.G., C.D., A.R.C., and B.G. are supported by FWO. The work of P.C. is supported by a Federal Government Belgium grant (IUAP7/03); long-term structural Methusalem funding by the Flemish Government; grants from the FWO and Foundation against Cancer; and a European Research Council Advanced Research grant (EU-ERC269073). X.L. is supported by the State Key Laboratory of Ophthalmology, Zhongshan Ophthalmic Center at the Sun Yat-Sen University and by the National Natural Science Foundation of China (81330021, 81670855).

AUTHOR CONTRIBUTIONS

U.B., F.M.-R., J.K., J.G., F.T., K.C.S.Q., C.D., A.R.C., R.C., S.L., E.T., V.C., K.B., L.-C.C., L.T., A. Staes, A. Sickmann, K.G., A.T., M.D., C.F.S., F.I., B.S., E.V., J.V.S., J.L.M., A.S., B.G., L.S., and M.M. contributed to the execution of certain experiments and/or analysis of the data, discussed the results, and commented on the manuscript. U.B., F.M.-R., and P.C. designed the experiments.

U.B., F.M.-R., X.L., and P.C. contributed to the execution, support, and analysis of experiments, data interpretation and/or advice, and wrote the paper. P.C. conceptualized and directed the study.

DECLARATION OF INTERESTS

The authors declare no competing interests.

REFERENCES

Aden, D.P., Fogel, A., Plotkin, S., Damjanov, I., and Knowles, B.B. (1979). Controlled synthesis of HBsAg in a differentiated human liver carcinomaderived cell line. Nature 282, 615–616.

Antoniewicz, M.R., Kelleher, J.K., and Stephanopoulos, G. (2007). Elementary metabolite units (EMU): a novel framework for modeling isotopic distributions. Metab. Eng. 9, 68–86.

Baeza, J., Smallegan, M.J., and Denu, J.M. (2016). Mechanisms and dynamics of protein acetylation in mitochondria. Trends Biochem. Sci. 41, 231–244.

Basu, S.S., and Blair, I.A. (2011). SILEC: a protocol for generating and using isotopically labeled coenzyme A mass spectrometry standards. Nat. Protoc. 7, 1–12.

Benedito, R., Roca, C., Sorensen, I., Adams, S., Gossler, A., Fruttiger, M., and Adams, R.H. (2009). The notch ligands Dll4 and Jagged1 have opposing effects on angiogenesis. Cell 137, 1124–1135.

Browne, C.D., Hindmarsh, E.J., and Smith, J.W. (2006). Inhibition of endothelial cell proliferation and angiogenesis by orlistat, a fatty acid synthase inhibitor. FASEB J. 20, 2027–2035.

Cailleau, R., Olive, M., and Cruciger, Q.V. (1978). Long-term human breast carcinoma cell lines of metastatic origin: preliminary characterization. In Vitro 14, 911–915.

Cantelmo, A.R., Conradi, L.C., Brajic, A., Goveia, J., Kalucka, J., Pircher, A., Chaturvedi, P., Hol, J., Thienpont, B., Teuwen, L.A., et al. (2016). Inhibition of the glycolytic activator PFKFB3 in endothelium induces tumor vessel normalization, impairs metastasis, and improves chemotherapy. Cancer Cell 30, 968–985.

Carmeliet, P., Moons, L., Luttun, A., Vincenti, V., Compernolle, V., De Mol, M., Wu, Y., Bono, F., Devy, L., Beck, H., et al. (2001). Synergism between vascular endothelial growth factor and placental growth factor contributes to angiogenesis and plasma extravasation in pathological conditions. Nat. Med. 7, 575–583.

Choudhary, C., Kumar, C., Gnad, F., Nielsen, M.L., Rehman, M., Walther, T.C., Olsen, J.V., and Mann, M. (2009). Lysine acetylation targets protein complexes and co-regulates major cellular functions. Science 325, 834–840.

Claxton, S., Kostourou, V., Jadeja, S., Chambon, P., Hodivala-Dilke, K., and Fruttiger, M. (2008). Efficient, inducible Cre-recombinase activation in vascular endothelium. Genesis 46, 74–80.

https://doi.org/10.1016/j.cmet.2018.07.019

Cohen, S.A., and Michaud, D.P. (1993). Synthesis of a fluorescent derivatizing reagent, 6-aminoquinolyl-N-hydroxysuccinimidyl carbamate, and its application for the analysis of hydrolysate amino acids via high-performance liquid chromatography. Anal. Biochem. 211, 279–287.
Colak, G., Pougovkina, O., Dai, L., Tan, M., Te Brinke, H., Huang, H., Cheng, Z., Park, J., Wan, X., Liu, X., et al. (2015). Proteomic and biochemical studies of lysine malonylation suggest its malonic aciduria-associated regulatory role in mitochondrial function and fatty acid oxidation. Mol. Cell. Proteomics 14, 3056–3071.
De Bock, K., Georgiadou, M., Schoors, S., Kuchnio, A., Wong, B.W., Cantelmo, A.R., Quaegebeur, A., Ghesquiere, B., Cauwenberghs, S., Eelen, G., et al. (2013). Role of PFKFB3-driven glycolysis in vessel sprouting. Cell 154, 651–663.
Du, Y., Cai, T., Li, T., Xue, P., Zhou, B., He, X., Wei, P., Liu, P., Yang, F., and Wei, T. (2015). Lysine malonylation is elevated in type 2 diabetic mouse models and enriched in metabolic associated proteins. Mol. Cell. Proteomics 14, 227–236.
Dunlop, E.A., Dodd, K.M., Seymour, L.A., and Tee, A.R. (2009). Mammalian target of rapamycin complex 1-mediated phosphorylation of eukaryotic initiation factor 4E-binding protein 1 requires multiple protein-protein interactions for substrate recognition. Cell. Signal. 21, 1073–1084.
Fendt, S.M., Bell, E.L., Keibler, M.A., Olenchock, B.A., Mayers, J.R., Wasylenko, T.M., Vokes, N.I., Guarente, L., Vander Heiden, M.G., and Stephanopoulos, G. (2013). Reductive glutamine metabolism is a function of the alpha-ketoglutarate to citrate ratio in cells. Nat. Commun. 4, 2236.
Fernandez, C.A., Des Rosiers, C., Previs, S.F., David, F., and Brunengraber, H. (1996). Correction of ^{13}C mass isotopomer distributions for natural stable isotope abundance. J. Mass Spectrom. 31, 255–262.
Gorsky, M.K., Burnouf, S., Dols, J., Mandelkow, E., and Partridge, L. (2016). Acetylation mimic of lysine 280 exacerbates human Tau neurotoxicity in vivo. Sci. Rep. 6, 22685.
Hou, X., Xu, S., Maitland-Toolan, K.A., Sato, K., Jiang, B., Ido, Y., Lan, F., Walsh, K., Wierzbicki, M., Verbeuren, T.J., et al. (2008). SIRT1 regulates hepatocyte lipid metabolism through activating AMP-activated protein kinase. J. Biol. Chem. 283, 20015–20026.
Huang, H., Vandekeere, S., Kalucka, J., Bierhansl, L., Zecchin, A., Bruning, U., Visnagri, A., Yuldasheva, N., Goveia, J., Cruys, B., et al. (2017). Role of glutamine and interlinked asparagine metabolism in vessel formation. EMBO J. 36, 2334–2352.
Hunt, D.A., Lane, H.M., Zygmont, M.E., Dervan, P.A., and Hennigar, R.A. (2007). MRNA stability and overexpression of fatty acid synthase in human breast cancer cell lines. Anticancer Res. 27, 27–34.
Jaffe, E.A., Nachman, R.L., Becker, C.G., and Minick, C.R. (1973). Culture of human endothelial cells derived from umbilical veins. Identification by morphologic and immunologic criteria. J. Clin. Invest. 52, 2745–2756.
Keydar, J., Gilead, Z., Hartman, J.R., and Ben-Shaul, Y. (1973). In vitro production of mouse mammary tumor virus in a mouse mammary tumor ascites line. Proc. Natl. Acad. Sci. USA 70, 2983–2987.
Kridel, S.J., Axelrod, F., Rozenkrantz, N., and Smith, J.W. (2004). Orlistat is a novel inhibitor of fatty acid synthase with antitumor activity. Cancer Res. 64, 2070–2075.
Kuda, O., Pietka, T.A., Demianova, Z., Kudova, E., Cvacka, J., Kopecky, J., and Abumrad, N.A. (2013). Sulfo-N-succinimidyl oleate (SSO) inhibits fatty acid uptake and signaling for intracellular calcium via binding CD36 lysine164: SSO also inhibits oxidized low density lipoprotein uptake by macrophages. J. Biol. Chem. 288, 15547–15555.
Kulkarni, R.A., Worth, A.J., Zengeya, T.T., Shrimp, J.H., Garlick, J.M., Roberts,A.M., Montgomery, D.C., Sourbier, C., Gibbs, B.K., Mesaros, C., et al. (2017). Discovering targets of non-enzymatic acylation by thioester reactivity profiling. Cell Chem. Biol. 24, 231–242.
Langmead, B., and Salzberg, S.L. (2012). Fast gapped-read alignment with Bowtie 2. Nat. Methods 9, 357–359.
Levenson, A.S., and Jordan, V.C. (1997). MCF-7: the first hormone-responsive breast cancer cell line. Cancer Res. 57, 3071–3078.
Meyer, J.G., D'Souza, A.K., Sorensen, D.J., Rardin, M.J., Wolfe, A.J., Gibson, B.W., and Schilling, B. (2016). Quantification of lysine acetylation and succinylation stoichiometry in proteins using mass spectrometric data-independent acquisitions (SWATH). J. Am. Soc. Mass Spectrom. 27, 1758–1771.
Michieli, P., Mazzone, M., Basilico, C., Cavassa, S., Sottile, A., Naldini, L., and Comoglio, P.M. (2004). Targeting the tumor and its microenvironment by a dual-function decoy Met receptor. Cancer Cell 6, 61–73.
Nakabayashi, H., Taketa, K., Miyano, K., Yamane, T., and Sato, J. (1982). Growth of human hepatoma cells lines with differentiated functions in chemically defined medium. Cancer Res. 42, 3858–3863.
Nishida, Y., Rardin, M.J., Carrico, C., He, W., Sahu, A.K., Gut, P., Najjar, R., Fitch, M., Hellerstein, M., Gibson, B.W., et al. (2015). SIRT5 regulates both cytosolic and mitochondrial protein malonylation with glycolysis as a major target. Mol. Cell 59, 321–332.
Olsen, J.V., Vermeulen, M., Santamaria, A., Kumar, C., Miller, M.L., Jensen, L.J., Gnad, F., Cox, J., Jensen, T.S., Nigg, E.A., et al. (2010). Quantitative phosphoproteomics reveals widespread full phosphorylation site occupancy during mitosis. Sci. Signal 3, ra3.
Peng, C., Lu, Z., Xie, Z., Cheng, Z., Chen, Y., Tan, M., Luo, H., Zhang, Y., He, W., Yang, K., et al. (2011). The first identification of lysine malonylation substrates and its regulatory enzyme. Mol. Cell. Proteomics 10, M111.012658.
Phoenix, T.N., Patmore, D.M., Boop, S., Boulos, N., Jacus, M.O., Patel, Y.T., Roussel, M.F., Finkelstein, D., Goumnerova, L., Perreault, S., et al. (2016). Medulloblastoma genotype dictates blood brain barrier phenotype. Cancer Cell 29, 508–522.
Pietrocola, F., Galluzzi, L., Bravo-San Pedro, J.M., Madeo, F., and Kroemer, G. (2015). Acetyl coenzyme A: a central metabolite and second messenger. Cell Metab. 21, 805–821.
Point, V., Benarouche, A., Zarrillo, J., Guy, A., Magnez, R., Fonseca, L., Raux, B., Leclaire, J., Buono, G., Fotiadu, F., et al. (2016). Slowing down fat digestion and absorption by an oxadiazolone inhibitor targeting selectively gastric lipolysis. Eur. J. Med. Chem. 123, 834–848.
Ritchie, M.E., Phipson, B., Wu, D., Hu, Y., Law, C.W., Shi, W., and Smyth, G.K. (2015). limma powers differential expression analyses for RNA-sequencing and microarray studies. Nucleic Acids Res. 43, e47. Robinson, M.D., McCarthy, D.J., and Smyth, G.K. (2010). edgeR: a Bioconductor package for differential expression analysis of digital gene expression data. Bioinformatics 26, 139–140.
Rohrig, F., and Schulze, A. (2016). The multifaceted roles of fatty acid synthesis in cancer. Nat. Rev. Cancer 16, 732–749.
Rosner, M., Siegel, N., Valli, A., Fuchs, C., and Hengstschlager, M. (2010). mTOR phosphorylated at S2448 binds to raptor and rictor. Amino Acids 38, 223–228.
Roudnicky, F., Poyet, C., Wild, P., Krampitz, S., Negrini, F., Huggenberger, R., Rogler, A., Stohr, R., Hartmann, A., Provenzano, M., et al. (2013). Endocan is upregulated on tumor vessels in invasive bladder cancer where it mediates VEGF-A-induced angiogenesis. Cancer Res. 73, 1097–1106.
Rysman, E., Brusselmans, K., Scheys, K., Timmermans, L., Derua, R., Munck, S., Van Veldhoven, P.P., Waltregny, D., Daniels, V.W., Machiels, J., et al. (2010). De novo lipogenesis protects cancer cells from free radicals and chemotherapeutics by promoting membrane lipid saturation. Cancer Res. 70, 8117–8126.
Saggerson, D. (2008). Malonyl-CoA, a key signaling molecule in mammalian cells. Annu. Rev. Nutr. 28, 253–272.
Saxton, R.A., and Sabatini, D.M. (2017). mTOR signaling in growth, metabolism, and disease. Cell 169, 361–371.
Schoors, S., Bruning, U., Missiaen, R., Queiroz, K.C., Borgers, G., Elia, I., Zecchin, A., Cantelmo, A.R., Christen, S., Goveia, J., et al. (2015). Fatty acid carbon is essential for dNTP synthesis in endothelial cells. Nature 520, 192–197.
Sharma, K., D'Souza, R.C., Tyanova, S., Schaab, C., Wisniewski, J.R., Cox, J., and Mann, M. (2014). Ultradeep human phosphoproteome reveals a distinct regulatory nature of Tyr and Ser/Thr-based signaling. Cell Rep. 8, 1583–1594.
Stone, K.R., Mickey, D.D., Wunderli, H., Mickey, G.H., and Paulson, D.F. (1978). Isolation of a human prostate carcinoma cell line (DU 145). Int. J. Cancer 21, 274–281.
Svensson, R.U., Parker, S.J., Eichner, L.J., Kolar, M.J., Wallace, M., Brun, S.N., Lombardo, P.S., Van Nostrand, J.L., Hutchins, A., Vera, L., et al. (2016). Inhibition of acetyl-CoA carboxylase suppresses fatty acid synthesis and tumor growth of non-small-cell lung cancer in preclinical models. Nat. Med. 22, 1108–1119.
Taddei, A., Giampietro, C., Conti, A., Orsenigo, F., Breviario, F., Pirazzoli, V., Potente, M., Daly, C., Dimmeler, S., and Dejana, E. (2008). Endothelial adherens junctions control tight junctions by VE-cadherin-mediated upregulation of claudin-5. Nat. Cell Biol. 10, 923–934.
Vazquez-Martin, A., Colomer, R., Brunet, J., Lupu, R., and Menendez, J.A. (2008). Overexpression of fatty acid synthase gene activates HER1/HER2 tyrosine kinase receptors in human breast epithelial cells. Cell Prolif. 41, 59–85.
Ventura, R., Mordec, K., Waszczuk, J., Wang, Z., Lai, J., Fridlib, M., Buckley, D., Kemble, G., and Heuer, T.S. (2015). Inhibition of de novo palmitate synthesis by fatty acid synthase induces apoptosis in tumor cells by remodeling cell membranes, inhibiting signaling pathways, and reprogramming gene expression. EBioMedicine 2, 808–824.

https://doi.org/10.1016/j.cmet.2018.07.019

Wei, X., Schneider, J.G., Shenouda, S.M., Lee, A., Towler, D.A., Chakravarthy, M.V., Vita, J.A., and Semenkovich, C.F. (2011). De novo lipogenesis maintains vascular homeostasis through endothelial nitric-oxide synthase (eNOS) palmitoylation. J. Biol. Chem. 286, 2933–2945.
Weinert, B.T., Moustafa, T., Iesmantavicius, V., Zechner, R., and Choudhary, C. (2015). Analysis of acetylation stoichiometry suggests that SIRT3 repairs nonenzymatic acetylation lesions. EMBO J. 34, 2620–2632.
Wenes, M., Shang, M., Di Matteo, M., Goveia, J., Martin-Perez, R., Serneels, J., Prenen, H., Ghesquiere, B., Carmeliet, P., and Mazzone, M. (2016). Macrophage metabolism controls tumor blood vessel morphogenesis and metastasis. Cell Metab. 24, 701–715.
Wragg, J.W., Finnity, J.P., Anderson, J.A., Ferguson, H.J., Porfiri, E., Bhatt, R.I., Murray, P.G., Heath, V.L., and Bicknell, R. (2016). MCAM and LAMA4 are highly enriched in tumor blood vessels of renal cell carcinoma and predict patient outcome. Cancer Res. 76, 2314–2326.
Yagasaki, R., Nakahara, T., Mori, A., Sakamoto, K., and Ishii, K. (2014a). Effects of mTOR inhibition on normal retinal vascular development in the mouse. Exp. Eye Res. 129, 127–134.
Yagasaki, R., Nakahara, T., Ushikubo, H., Mori, A., Sakamoto, K., and Ishii, K. (2014b). Anti-angiogenic effects of mammalian target of rapamycin inhibitors in a mouse model of oxygen-induced retinopathy. Biol. Pharm. Bull. 37, 1838–1842.
Yang, C.S., Matsuura, K., Huang, N.J., Robeson, A.C., Huang, B., Zhang, L., and Kornbluth, S. (2015). Fatty acid synthase inhibition engages a novel caspase-2 regulatory mechanism to induce ovarian cancer cell death. Oncogene 34, 3264–3272.
Zaidi, N., Lupien, L., Kuemmerle, N.B., Kinlaw, W.B., Swinnen, J.V., and Smans, K. (2013). Lipogenesis and lipolysis: the pathways exploited by the cancer cells to acquire fatty acids. Prog. Lipid Res. 52, 585–589.